Asymmetry of spin wave dispersions in a hexagonal magnonic crystal

F. Montoncello, S. Tacchi, L. Giovannini, M. Madami, G. Gubbiotti, G. Carlotti, E. Sirotkin, E. Ahmad, F. Y. Ogrin, and V. V. Kruglyak

Citation: Applied Physics Letters **102**, 202411 (2013); doi: 10.1063/1.4807657
View online: http://dx.doi.org/10.1063/1.4807657
View Table of Contents: http://scitation.aip.org/content/aip/journal/apl/102/20?ver=pdfcov
Published by the AIP Publishing

Asymmetry of spin wave dispersions in a hexagonal magnonic crystal

F. Montoncello,[1,a)] S. Tacchi,[2] L. Giovannini,[1] M. Madami,[2] G. Gubbiotti,[3] G. Carlotti,[2] E. Sirotkin,[4] E. Ahmad,[4] F. Y. Ogrin,[4] and V. V. Kruglyak[4]
[1]*Dipartimento di Fisica e Scienze della Terra, CNISM-University of Ferrara, Ferrara, Italy*
[2]*Dipartimento di Fisica, CNISM-University of Perugia, Perugia, Italy*
[3]*Istituto Officina dei Materiali del Consiglio Nazionale delle Ricerche (IOM-CNR), Sede di Perugia, c/o Dipartimento di Fisica, Perugia, Italy*
[4]*School of Physics, University of Exeter, Exeter, United Kingdom*

(Received 3 October 2012; accepted 1 May 2013; published online 24 May 2013)

We report a study of the dispersion of spin waves in a hexagonal array of interacting ferromagnetic nanodisks for two orthogonal orientations of the in-plane applied magnetic field, i.e., either parallel or perpendicular to the direction of first neighbour disks. The experimental data were modelled using the dynamical matrix method, and the results were interpreted in terms of the effective wave vector model. We have found that spin waves propagating in the two orthogonal directions exhibit marked asymmetry concerning the existence of maxima/minima in their dispersion curves and the sign of their group velocities. © *2013 AIP Publishing LLC*. [http://dx.doi.org/10.1063/1.4807657]

Magnonic crystals (MCs) are artificial materials with periodic modulation of magnetic properties where the spin wave (SW) band structure can be tailored and controlled.[1–8] This tunability makes MCs promising candidates for creation of versatile devices such as adjustable filters and waveguides operating in the microwave frequency range.[3,5,9,10]

Dense arrays of in-plane magnetized nano-disks have been extensively investigated by ferromagnetic resonance,[11–15] Brillouin light scattering (BLS),[16–23] and time resolved magneto-optical measurements.[24–28] However, arrays of disks arranged into a hexagonal mesh have been sparsely studied so far, and the experimental data have been presented for wave vector $k = 0$ only.[29] This is probably due to the fact that arrays of disks arranged in the hexagonal symmetry are challenging not only from the fabrication and characterization perspective but also from the point of view of their theoretical modeling.[6,8,9,11,24,25,30,31]

In this work, we study the dispersion of collective SWs in the Voigt scattering geometry in a hexagonal array of 20 nm thick Permalloy ($Ni_{80}Fe_{20}$) disks for two different directions of the applied magnetic field and therefore SW propagation. We find that equivalent modes in equivalent scattering geometries have different dispersive behavior ("asymmetry") along the two principal directions of the lattice. The array of disks has been fabricated by the etched nano-sphere lithography technique.[32,33] The disks have average diameter of (378 ± 2) nm and formed an array of (390 ± 3) nm periodicity. The scanning electron micrographs (SEM) of the array (Figs. 1(a) and 1(b)) demonstrate a well-defined arrangement of disks, with uniform spacing and good edge definition.[34] However, a detailed investigation of the SEM images at different magnification revealed that the orientation of the symmetry axis suffers a decrease of 25° over the distance of 5.0 mm.[35]

The BLS experiments were performed in the Voigt configuration, where the in-plane transferred wave-vector ($\mathbf{k}$) was perpendicular to the external magnetic field applied in the sample plane. The SW dispersion was measured for two different orientations of the magnetic field of $\mu_0 H = 40$ mT, as indicated in Figs. 1(a) and 1(b). For the field applied along the direction of nearest-neighbor disks (x-axis direction) k varied in ΓM, while for the field applied perpendicularly to the direction of nearest-neighbor disks (y-axis direction) k varied in ΓM′. The BLS spectra were recorded in the back-scattering configuration, by sweeping the SW wave vector k up to 1.6×10^5 rad/cm.[36]

In the simulations, the equilibrium configuration of the system was computed by OOMMF[37] on a finite sample of 17 disks displaced into a hexagonal lattice with the edge-to-edge separation of 24 nm (see Fig. 1(c)). The central disk was used as primitive cell with oblique coordinates. Each disk had diameter of 376 nm and thickness of 20 nm and was discretized into micromagnetic cells of dimensions $4\,\text{nm} \times 4\,\text{nm} \times 20\,\text{nm}$. Then, the dynamical matrix method (DMM) was used to calculate frequencies and spatial profiles of all modes in the magnonic spectrum as a function of the Bloch wavevector.[38] At each k, the BLS cross section was also calculated for each mode profile[39,40] and compared with the measured intensities. A comparison of the calculated and measured mode frequencies and cross-sections was used to identify the modes, which were then labeled according to the scheme described in Ref. 18. The dynamic magnetization of each mode (Bloch wave) can be interpreted using the expression $\delta\mathbf{m}(\mathbf{r}) = \delta\tilde{\mathbf{m}}_k(\mathbf{r})e^{i\mathbf{k}\cdot\mathbf{r}}$, where $\mathbf{r}$ is the radius-vector in the direct space, $\mathbf{k}$ is the Bloch wave vector, and $\delta\tilde{\mathbf{m}}_k$ is the cell function, which has the periodicity of the array. The magnetic parameters assumed in the calculations were $A = 1.0 \times 10^{11}$ J/m for the exchange stiffness parameter, $M_s = 650 \times 10^5$ A/m for the saturation magnetization, and $\gamma/2\pi = 29.5$ GHz/T for the reduced gyromagnetic ratio. In the calculations, the external field was assumed to be (exactly) parallel either to x- or y-axis (Figs. 1(c) and 1(d)). The BLS intensity depends on the real part of the out-of-plane (z) component of the dynamic magnetization of the mode in a single cell (which depends on k) and on the light incidence angle θ_i.

When $\mathbf{H}$ is parallel to the direction of nearest-neighbor disks (i.e., along x-axis), the magnetization is in a "leaf"

a)Author to whom correspondence should be addressed. Electronic mail: montoncello@fe.infn.it

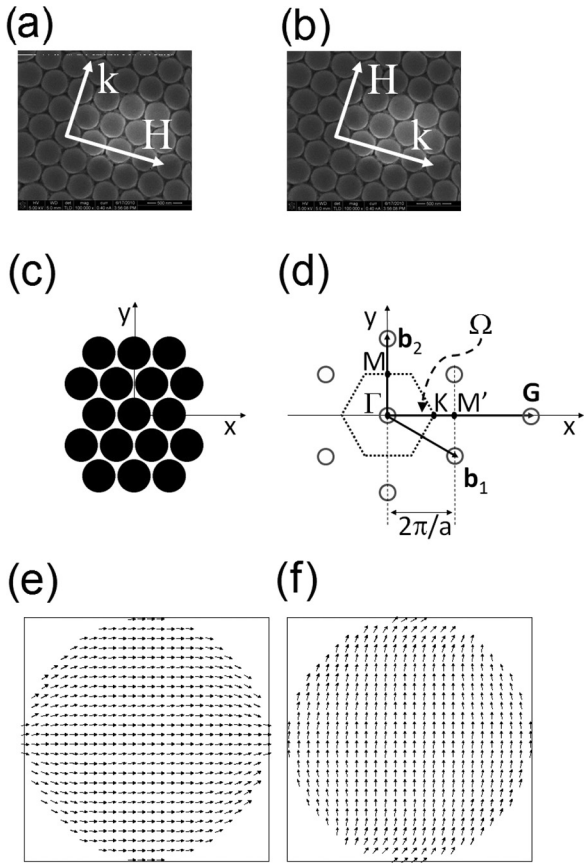

FIG. 1. Panels (a) and (b): SEM images of the array with indication of **k** and **H** in the two cases under consideration. Panel (c): lattice points in the direct space; *x*-axis is taken along the direction of nearest-neighbor disks. Panel (d): lattice points in the reciprocal space, $\mathbf{b}_1$ and $\mathbf{b}_2$ are the primitive vectors; dotted line marks the first Brillouin zone; vector $\mathbf{G}=2\mathbf{b}_1+\mathbf{b}_2$ indicates a lattice point equivalent to Γ. Schematic representation of the equilibrium magnetic configurations at the field $\mu_0 H = 40\,\text{mT}$, applied parallel (panel (e)) or perpendicular (panel (f)) to the direction of nearest-neighbor disks.

configuration (Fig. 1(e)). In this case, the plane of incidence is taken parallel to *y*-direction, so that **k** is varied along ΓM. As shown in Fig. 1(d), M is a "mirror point" for frequency. In contrast, when **H** is perpendicular to the direction of nearest-neighbor disks (i.e., along the *y*-axis) and **k** is varied along ΓM′ direction (i.e., along *x*-axis), the mirror point for frequency is not at the zone boundary (K) but is found at the M′ point. Also, the magnetization in each disk now forms an "S"-state (Fig. 1(f)). The curling of the magnetization is due to the fact that magnetic poles at the ends of nearest-neighbor disks (which are misaligned along y) create curled field lines to which magnetic moments align.

To interpret the dispersion of different modes, Tacchi *et al.*[18] introduced a 2-D effective wave vector $\mathbf{k}_{\text{eff}}$, which includes and replaces both the band index and the Bloch wave vector. The effective wave vector represents the overall oscillation of the magnetization across the array, because it takes into account both the oscillation within individual disks due to the mode character (i.e., due to the number and orientation of nodal lines) and the variation between adjacent dots due to the Bloch factor, $e^{i\mathbf{k}\cdot\mathbf{r}}$. In the 2-D case, $\mathbf{k}_{\text{eff}}$ has two components, parallel and perpendicular to the applied field. The former component is associated with the backward ("BA") character of the spin wave (in terms of the dispersion of magnetostatic spin waves) and is therefore denoted as $\mathbf{k}_{\text{BA}}$, while the latter component is associated with the Damon-Eshbach ("DE") character and is therefore denoted as $\mathbf{k}_{\text{DE}}$. Overall, this gives $\mathbf{k}_{\text{eff}}=\mathbf{k}_{\text{BA}}+\mathbf{k}_{\text{DE}}$. Both $\mathbf{k}_{\text{BA}}$ and $\mathbf{k}_{\text{DE}}$ increase as the number of nodal lines perpendicular and parallel to the applied magnetic field increases, respectively. The nodal lines can be "actual" (i.e., occurring within the disk) or "effective" (i.e., occurring between adjacent disks, as a consequence of Bloch phase change). Since the disks within the array are coupled by the dipolar interaction, we can map $\mathbf{k}_{\text{eff}}$ on the well-known dispersions of the magnetostatic spin waves to predict the overall behavior of the frequency of any given mode as a function of $\mathbf{k}_{\text{BA}}$ and $\mathbf{k}_{\text{DE}}$. If $\mathbf{k}_{\text{BA}}$ ($\mathbf{k}_{\text{DE}}$) increases, the mode frequency decreases (increases) and vice versa (see, e.g., Ref. 18 for details).

Due to the peculiar hexagonal symmetry of the lattice, the dispersion curves are characterized by interesting features not present, e.g., in square arrays. We first consider the case of **H** applied parallel to *x*-axis, and hence **k** is along ΓM (Figs. 1(a) and 1(d)). In Table I, the Bloch factor is computed for $\mathbf{k}=(0,0)$, i.e., Γ, and $\mathbf{k}=(0,\frac{2\pi}{\sqrt{3}a})$, i.e., M, for the 6 lattice points around $\mathbf{r}=(0,0)$. According to this table, we can understand the behavior of $\mathbf{k}_{\text{eff}}$ plotting the phase relationship among nearest neighbor disks for a few modes (Fig. 2, left panel), using the Bloch relation $\delta\mathbf{m}(\mathbf{r}+\mathbf{R})=\delta\mathbf{m}(\mathbf{r})e^{i\mathbf{k}\cdot\mathbf{R}}$, where **R** is any lattice point in direct space. In Figs. 2 and 3 we show only the real part of the out-of-plane (*z*) component of $\delta\mathbf{m}(\mathbf{r})$, although the considerations below apply equally to its imaginary part.

Note that $\mathbf{k}_{\text{BA}}$ does not vary along ΓM for any of the modes. Conversely, $\mathbf{k}_{\text{DE}}$ increases for the fundamental mode and for 1-DE (as well as for any *n*-DE with odd *n*) but decreases for any *n*-DE with even *n*.[18] Due to the misalignments of neighbor disks along *y* direction, the effective wave vector variation for *m*-BA modes depends also on *m*. We checked that if *p* is a nonzero integer, *m*-BA modes with $m=4p$-3 and $m=4p$-2 have a negative frequency dispersion, instead with $m=4p$-1 and $m=4p$ have a positive frequency dispersion; of course, the bandwidth amplitude decreases as *m* increases.

In Fig. 3(a) we plot both experimental (symbols) and calculated (lines) dispersions: the line thickness indicates the calculated BLS cross section, which can be large (bold line), average (straight line), or negligible (dotted line). The overall agreement is good, apart from the slight asymmetry in the measured frequency of the fundamental mode, which can be either attributed to a few-degree-misalignment of the applied magnetic field with respect to the nominal direction of the array or to the above mentioned variation of the symmetry axis orientation within the sample.[41] Furthermore, an appreciable frequency downshift of the end mode (indicated with "EM (round)"), with respect to the calculated value, is observed. This mode is strongly localized near the disk

TABLE I. Values of the Bloch factor at Γ and M.

	$\mathbf{R}=(0,0)$	$\mathbf{R}=(\pm a,0)$	$\mathbf{R}=\left(\frac{\pm a}{2},\frac{\pm\sqrt{3}a}{2}\right)$
Γ:$\mathbf{k}=(0,0)$	1	1	1
M:$\mathbf{k}=\left(0,\frac{2\pi}{\sqrt{3}a}\right)$	1	1	−1

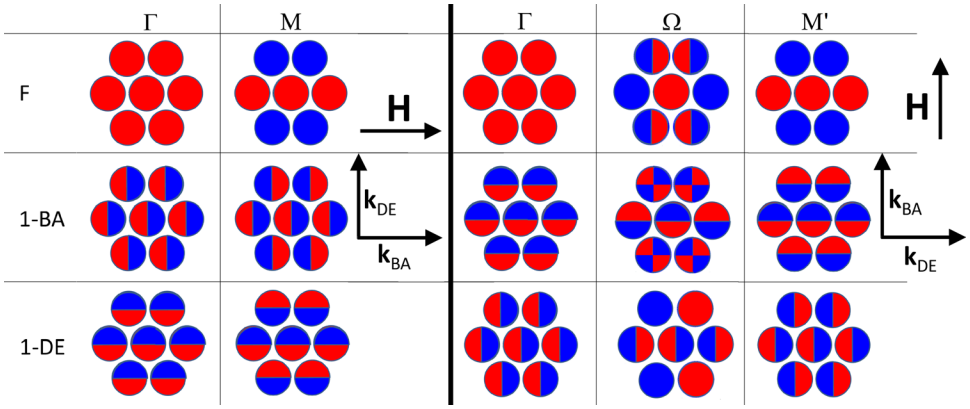

FIG. 2. Schematic view of the phase relationship among nearest-neighbor dots at different values of the Bloch wave vector along y (left panel) and x (right panel), with reference to the real part of the out-of-plane component of the dynamic magnetization. The red and blue colors mean that the Bloch factor is 1 and −1, respectively. In the lattice points where the Bloch factor is $\pm i$, the profile changes symmetry (see Tables I and II). This helps in finding the behavior of $\mathbf{k}_{DE}$ and $\mathbf{k}_{BA}$.

boundaries, and so the discrepancies are likely to result from the slightly different edge details in the model and real disks, both in terms of the geometry and magnetic configuration.[21] To verify this point, we repeated the calculations for disks with ends flattened in the direction perpendicular to the applied magnetic field. This hypothesis is suggested by the inspection of the SEM images reported in Figs. 1(a) and 1(b) where the edge flattening is clearly visible. We observed that the flattening decreases the frequency of the end mode and thereby improves the agreement with the experiment ["EM (flat)"]. One of the insets in Fig. 3(a) shows the profile of the end mode in the disk with flattened ends. The oscillation region for the end mode is very narrow, and so the associated dynamic coupling fields are small, and the corresponding dispersion curve is almost flat. It is noteworthy that the flattening of the disk edges does not influence the frequency of modes localized in the disks center. Finally, we show a mixed mode (2-BA × 1-DE), whose calculated frequency increases up to the maximum at M (magnonic band amplitude of 0.3 GHz), as can be predicted by the effective wave vector variation (not shown in Fig. 2). Measurements do not fit exactly this trend, probably because the experimental error is comparable with the mode bandwidth.

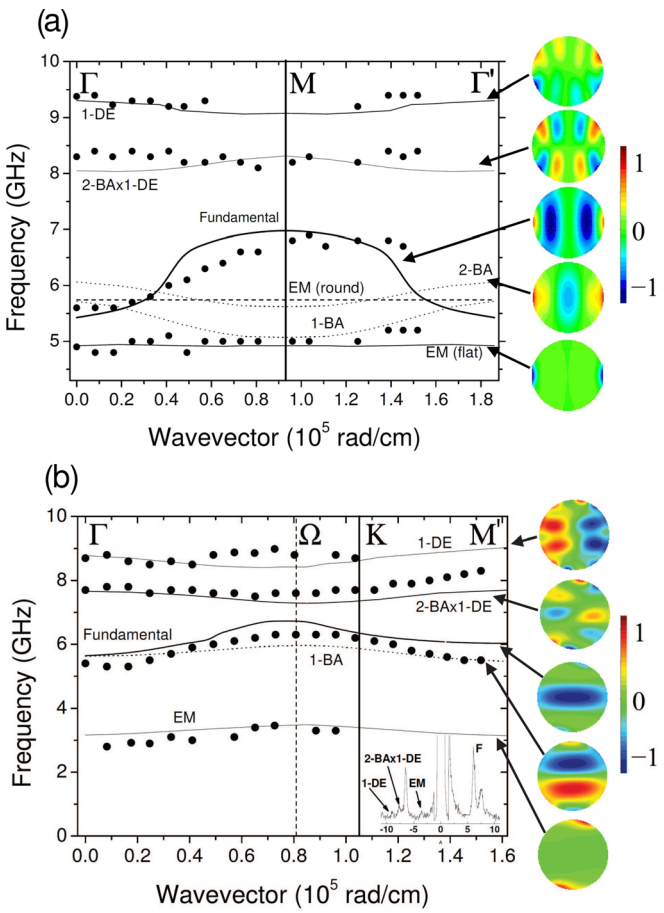

FIG. 3. Experimental (symbols) and calculated (lines) SW dispersions along (a) the ΓM and (b) ΓM′ directions. In panel (a) the vertical line at 0.93×10^5 rad/cm denotes the M point. Dotted lines are (BLS-inactive) backward-like modes with one (1-BA) and two (2-BA) nodes. Dashed line corresponds to the frequency of the EM calculated for a disk with rounded ends, to compare with the one calculated for a disk with flattened ends, indicated as "EM (flat)" and shown in the inset at the bottom-right. In panel (b) the zone boundary is at $4\pi/3\,a = 1.05 \times 10^5$ rad/cm, corresponding to K point. Ω is the middle point of ΓM′. Insets show the real z-component of the dynamic magnetization. Figure insets show a representative BLS spectrum measured at $k_x = 0.73 \times 10^5\,\mathrm{cm}^{-1}$. In both panels, insets show the real z-component of the dynamic magnetization.

Now, we consider the case of **H** parallel to the y-axis. In this case, the Bloch wave vector **k** is along x-axis, i.e., along ΓM′ (Figs. 1(b) and 1(d)). Hence, $\mathbf{k}_{BA}$ is along y-axis, and $\mathbf{k}_{DE}$ is along x-axis. This configuration shows a very interesting feature, peculiar to the concurrence of hexagonal symmetry and magnetism. Indeed, we considered an additional (non-conventional) point Ω in the reciprocal space, located in the middle of ΓM′, i.e., at $\mathbf{k} = (\frac{\pi}{a},0)$ (Fig. 1(d)). For in-plane magnetized samples, δm_z is completely real at Γ ($\mathbf{k} = 0$), but moving from Γ, δm_z is in general complex (i.e., with real and imaginary parts). In particular, at Ω, the Bloch factor calculated for $\mathbf{R} = (\pm a/2,0)$ equals the imaginary unit (Table II). Hence, in those lattice points, the real and imaginary parts of δm_z are exchanged. This results in a change of symmetry (i.e., of the number of nodal lines) with respect to those at $\mathbf{R} = (0,0)$. Recalling that in Fig. 2 only the real part is shown, it is possible to see (Fig. 2, right panel) that moving from Γ to Ω, $\mathbf{k}_{DE}$ of the fundamental mode increases, while $\mathbf{k}_{BA}$ is constant. Hence, according to the magnetostatic dispersion, the joint effect is a frequency increase. Moving from Ω to M′,

TABLE II. Values of the Bloch factor at Γ, M′, and the middle point Ω. i is the imaginary unit.

	$\mathbf{R} = (0,0)$	$\mathbf{R} = (\pm a,0)$	$\mathbf{R} = \left(\pm\frac{a}{2},\frac{\sqrt{3}a}{2}\right)$	$\mathbf{R} = \left(\pm\frac{a}{2},-\frac{\sqrt{3}a}{2}\right)$
Γ:$\mathbf{k} = (0,0)$	1	1	1	1
Ω:$\mathbf{k} = (\frac{\pi}{a},0)$	1	−1	$\pm i$	$\pm i$
M′:$\mathbf{k} = \left(\frac{2\pi}{a},0\right)$	1	1	−1	−1

instead, $\mathbf{k}_{DE}$ of the fundamental mode decreases (and this implies a frequency decrease), while $\mathbf{k}_{BA}$ increases (and this also implies a frequency decrease). Hence, the joint effect is a frequency decrease. Conversely, concerning the 1-DE mode, it can be seen that from Γ to Ω $\mathbf{k}_{DE}$ decreases while $\mathbf{k}_{BA}$ is constant. Hence, the joint effect is a frequency decrease. Instead, from Ω to M′, $\mathbf{k}_{DE}$ increases while $\mathbf{k}_{BA}$ decreases, and both variations concur to a frequency increase. It can be shown that, for *n*-DE modes with other odd *n*, the situation is the same, while for even *n*, it is opposite. For *m*-BA modes, instead, independently of *m*, $\mathbf{k}_{DE}$ increases from Γ to Ω, while $\mathbf{k}_{BA}$ is constant. Hence, the combined effect is a frequency increase. When considering dispersion from Ω to M′, both $\mathbf{k}_{DE}$ and $\mathbf{k}_{BA}$ decrease, and the joint effect is less trivial in this case, because the frequency decrease due to the $\mathbf{k}_{DE}$ variation contrasts the increase due to the $\mathbf{k}_{BA}$ variation. In our case, the former effect dominates, and the overall behavior is a frequency decrease

Due to the different variations of $\mathbf{k}_{DE}$ and $\mathbf{k}_{BA}$ before and after Ω, the frequency curves of each mode are not exactly symmetric with respect to this point, which therefore does not represent a mirror symmetry point for the SW dispersion. Summarizing, Ω is always a maximum for the fundamental, *m*-BA, and for the even *n*-DE modes, and a minimum for odd *n*-DE modes (apart from computational/experimental errors). We stress that this feature is peculiar to the concurrence of hexagonal symmetry and magnetism (which has, intrinsically, an axial symmetry), and therefore it could not be observed for square arrays. Due to the S-state configuration, higher order modes happen to be more easily hybridized (or distorted). Hence, the variation of $\mathbf{k}_{eff}$ is more difficult to evaluate and does not always follow the above simple rules (which are rigorously valid within the stationary wave picture[42] of the cell functions).

In Fig. 3(b), we plot both the experimental (symbols) and calculated (lines) dispersions for the dominant BLS active modes, showing a good agreement. Note that the behavior of the end mode (EM) is very similar to that of F mode (maximum in Ω) and that the EM bandwidth is greater than in the case of **H** parallel to *x*-axis. This is because, due to the curled static magnetization, the oscillation region is wider in this case, and the associated dynamic coupling fields are therefore greater.

In conclusion, the SW dispersion in a hexagonal array of disks has been investigated by means of the BLS technique in the Voigt geometry, for the in-plane magnetic field applied along the two main symmetry directions, which are mutually orthogonal. We have found that equivalent modes in equivalent (Voigt) scattering geometries can behave differently along the two orthogonal directions ("asymmetry"). In particular, the existence of a maximum/minimum (i.e., zero group velocity) before zone boundary has been observed when the wave vector is perpendicular to the direction of nearest neighbor disks, but not when it is parallel to this direction. Our findings can be useful for applications in magnonics and spintronics, e.g., for waveguides where the direction, speed, and bandwidth of the signal can be tuned by a simple rotation of the applied field and for spin-logic devices, where positive/negative dispersions can be associated with the propagation direction of the signal and therefore with different binary digits.

This work was supported by the European Community's Seventh Framework Programme (FP7/2007-2013) under Grant Agreement Nos. 228673 (MAGNONICS) and 233552 (DYNAMAG) and by MIUR-PRIN 2010-11 Project 2010ECA8P3 "DyNanoMag." V.V.K. also acknowledges funding received from EPSRC of the UK under project EP/E055087/1.

[1]M. Krawczyk, J.-C. Lévy, D. Mercier, and H. Puszkarski, Phys. Lett. A **282**, 186 (2001).
[2]S. A. Nikitov, Ph. Tailhades, and C. S. Tsai, J. Magn. Magn. Mater. **236**, 320 (2001).
[3]V. V. Kruglyak, S. O. Demokritov, and D. Grundler, J. Phys. D: Appl. Phys. **43**, 264001 (2010).
[4]B. Lenk, H. Ulrichs, F. Garbs, and M. Münzenberg, Phys. Rep. **507**, 107 (2011).
[5]A. V. Chumak, V. I. Vasyuchka, A. A. Serga, M. P. Kostylev, V. S. Tiberkevich, and B. Hillebrands, Phys. Rev. Lett. **108**, 257207 (2012).
[6]R. Verba, G. Melkov, V. Tiberkevich, and A. Slavin, Appl. Phys. Lett. **100**, 192412 (2012).
[7]*Magnonics: From Fundamental to Applications, Topics in Applied Physics*, edited by S. O. Demokritov and A. N. Slavin (Springer, 2013), Vol. 125.
[8]F. Montoncello and L. Giovannini, Appl. Phys. Lett. **100**, 182406 (2012).
[9]R. Huber and D. Grundler, Proc. SPIE **8100**, 81000D (2011).
[10]A. Khitun, M. Bao, and K. L. Wang, J. Phys. D: Appl. Phys. **43**, 264005 (2010).
[11]S. Jung, B. Watkins, L. De Long, J. B. Ketterson, and V. Chandrasekhar, Phys. Rev. B **66**, 132401 (2002).
[12]I. P. Nevirkovets, O. Chernyashevskyy, J. B. Ketterson, V. Metlushko, and B. K. Sarma, J. Appl. Phys. **104**, 063920 (2008).
[13]S. Jain, M. Kostylev, and A. O. Adeyeye, Phys. Rev. B **82**, 214422 (2010).
[14]M. Kostylev, R. Magaraggia, F. Y. Ogrin, E. Sirotkin, V. F. Mescheryakov, N. Ross, and R. L. Stamps, IEEE Trans. Magn. **44**, 2741 (2008).
[15]H. J. Chia, F. Guo, L. M. Belova, and R. D. McMichael, Appl. Phys. Lett. **101**, 042408 (2012).
[16]G. Gubbiotti, S. Tacchi, M. Madami, G. Carlotti, A. O. Adeyeye, and M. Kostylev, J. Phys. D: Appl. Phys. **43**, 264003 (2010).
[17]C. Mathieu, C. Hartmann, M. Bauer, O. Buettner, S. Riedling, B. Roos, S. O. Demokritov, B. Hillebrands, B. Bartenlian, C. Chappert, D. Decanini, F. Rousseaux, E. Cambril, A. Müller, B. Hoffmann, and U. Hartmann, Appl. Phys. Lett. **70**, 2912 (1997).
[18]S. Tacchi, F. Montoncello, M. Madami, G. Gubbiotti, G. Carlotti, L. Giovannini, R. Zivieri, F. Nizzoli, S. Jain, A. O. Adeyeye, and N. Singh, Phys. Rev. Lett. **107**, 127204 (2011).
[19]S. Tacchi, G. Duerr, J. W. Klos, M. Madami, S. Neusser, G. Gubbiotti, G. Carlotti, M. Krawczyk, and D. Grundler, Phys. Rev. Lett. **109**, 137202 (2012).
[20]G. Gubbiotti, M. Madami, S. Tacchi, G. Carlotti, G. Socino, and T. Okuno, Surf. Sci. **600**, 4143 (2006).
[21]H. T. Nembach, J. M. Shaw, T. J. Silva, W. L. Johnson, S. A. Kim, R. D. McMichael, and P. Kabos, Phys. Rev. B **83**, 094427 (2011).
[22]F. Montoncello, L. Giovannini, F. Nizzoli, H. Tanigawa, T. Ono, G. Gubbiotti, M. Madami, S. Tacchi, and G. Carlotti, Phys. Rev. B **78**, 104421 (2008).
[23]S. Tacchi, M. Madami, G. Gubbiotti, G. Carlotti, H. Tanigawa, T. Ono, and M. P. Kostylev, Phys. Rev. B **82**, 024401 (2010).
[24]P. S. Keatley, V. V. Kruglyak, A. Neudert, E. A. Galaktionov, R. J. Hicken, J. R. Childress, and J. A. Katine, Phys. Rev. B **78**, 214412 (2008).
[25]V. V. Kruglyak, P. S. Keatley, A. Neudert, R. J. Hicken, J. R. Childress, and J. A. Katine, Phys. Rev. Lett. **104**, 027201 (2010).
[26]B. Rana, D. Kumar, S. Barman, S. Pal, Y. Fukuma, Y. Otani, and A. Barman, ACS Nano **5**, 9559 (2011).
[27]Z. Liu, R. Brandt, Y. Yahagi, B. Hansen, B. Harteneck, J. Bokor, A. R. Hawkins, and H. Schmidt, Appl. Phys. Lett. **98**, 052502 (2011).
[28]B. Rana, D. Kumar, S. Barman, S. Pal, R. Mandal, Y. Fukuma, Y. Otani, S. Sugimoto, and A. Barman, J. Appl. Phys. **111**, 07D503 (2012).
[29]N. Ross, M. Kostylev, and R. L. Stamps, J. Appl. Phys. **109**, 013906 (2011).
[30]C. C. Dantas, Physica E **44**, 675 (2011).

[31]R. Rückriem, P. Krone, T. Schrefl, and M. Albrecht, Appl. Phys. Lett. **100**, 242402 (2012).
[32]S. M. Weekes, F. Y. Ogrin, W. A. Murray, and P. S. Keatley, Langmuir **23**, 1057 (2007).
[33]E. Sirotkin and F. Y. Ogrin, IEEE Trans. Magn. **46**, 1840 (2010).
[34]E. Sirotkin, J. D. Apweiler, and F. Y. Ogrin, Langmuir **26**, 10677 (2010).
[35]E. K. Semenova, F. Montoncello, S. Tacchi, G. Dürr, E. Sirotkin, E. Ahmad, M. Madami, G. Gubbiotti, S. Neusser, D. Grundler, F. Y. Ogrin, R. J. Hicken, V. V. Kruglyak, D. V. Berkov, and N. L. Gorn, "Magnetodynamical response of large-area close-packed arrays of circular dots fabricated by nanosphere lithography," Phys. Rev. B (to be published).
[36]G. Carlotti and G. Gubbiotti, Riv. Nuovo Cimento **22**, 1 (1999).
[37]M. Donahue and D. G. Porter, *OOMMF User's Guide*, Version 1.0, Interagency Report NISTIR 6376 (NIST, Gaithersburg, MD, USA, 1999).
[38]L. Giovannini, F. Montoncello, and F. Nizzoli, Phys. Rev. B **75**, 024416 (2007).
[39]R. Zivieri, F. Montoncello, L. Giovannini, F. Nizzoli, S. Tacchi, M. Madami, G. Gubbiotti, G. Carlotti, and A. O. Adeyeye, Phys. Rev. B **83**, 054431 (2011).
[40]G. Gubbiotti, G. Carlotti, T. Okuno, M. Grimsditch, L. Giovannini, F. Montoncello, and F. Nizzoli, Phys. Rev. B **72**, 184419 (2005).
[41]Consider that changing in the value of the in-plane wavevector in Fig. 3 implicates a rotation of the sample, causing an unavoidable small change in the sample region probed by the laser spot.
[42]F. Montoncello and F. Nizzoli, J. Appl. Phys. **107**, 023906 (2010).